Materials Horizons

Atomically Precise Alloy AgCu Cuboid Nanocluster with Cubic Core: Gram Scale Synthesis, Total Structure, Electronic Structure, and Catalytic Performance

Journal:	*Materials Horizons*
Manuscript ID	MH-COM-09-2024-001324.R3
Article Type:	Communication
Date Submitted by the Author:	05-Apr-2025

Complete List of Authors:	Nag, Abhijit; Khalifa University Butt, Abdul Mannan ; Khalifa University of Science and Technology, Chemistry Yang, Moon Young; Korea Advanced Institute of Science and Technology, Materials Science and Engineering Managutti, Praveen; Khalifa University of Science and Technology, Chemistry Masood, Bilal; Khalifa University of Science and Technology Haja Mohideen, Mohamed Infas; Khalifa University of Science and Technology, Chemistry Abdelhady, Ahmed; Khalifa University, Chemistry Abu Haija, Mohammad; Khalifa University, Mohamed, Sharmarke; Khalifa University of Science Technology, Department of Chemistry Merinov, Boris; California Institute of Technology, Chemistry and Chemical Engineering Goddard III, William; California Institute of Technology, Qurashi, Ahsanulhaq; King Fahd University of Petroleum and Minerals,

Note: The following files were submitted by the author for peer review, but cannot be converted to PDF. You must view these files (e.g. movies) online.

Manuscript_(4).docx

In modern synthetic chemistry, ligand-protected atomically precise metal alloy nanoclusters are of great interest due to their unique physiochemical properties and specific molecular structure, making them an excellent platform for researching structure-activity relationships at the atomic scale. Unlike the rapid expansion of gold and silver alloy clusters, the easy oxidation of copper poses a challenge in the synthesis of stable copper and silver alloy clusters. As a result, the development of a large-scale synthesis and stable copper and silver alloy nanocluster with a defined metal core is much more challenging. This work introduces the total structure and gram scale synthesis of a stable and highly symmetric 2-phenylethanethiol (PETH) and triphenylphosphine (TPP)-protected AgCu alloy nanocluster $[Ag_4Cu_{28}H_6(PET)_{16}Cl_8(TPP)_8][BF_4]_2$ with a cuboid shape having cubic metal core, via a facile one-pot reduction method. Furthermore, the nanocluster has remarkable catalytic activity ($k = 7.86\ min^{-1}$) for hydrogenating dangerous nitroarenes. The nanocluster exhibited a notably greater catalytic efficiency in comparison to alternative copper hydride nanocluster catalysts. The synthesis of pure AgCu alloy nanocluster, which can be produced in large quantities (up to 1.112 g of pure crystals in one pot), can now be studied in detail, opening up new avenues for applications.

Data availability statements

The manuscript does not include:

- No Software codes used
- Crystallographic data files are provided
- No primary research results, software or code have been included.
- The detailed results of this article have been included as part of the Supplementary Information for publication.

Atomically Precise Alloy AgCu Cuboid Nanocluster with Cubic Core: Gram Scale Synthesis, Total Structure, Electronic Structure, and Catalytic Performance

Abhijit Nag[†, ‡], Abdul Mannan Butt[†, ‡], Moon Young Yang[§], Praveen B. Managutti[‡, #], Bilal Masood Pirzada[‡], M. Infas H. Mohideen [†, ‡], Ahmed L. Abdelhady[†, ‡], Mohamed Abu Haija[†, ‡], Sharmarke Mohamed[†, ‡, #], Boris V. Merinov[§], William A. Goddard III[§] and Ahsanulhaq Qurashi[†, ‡*]*

[†] Department of Chemistry, Khalifa University of Science and Technology, Abu Dhabi 127788, UAE

[‡] Center for Catalysis and Separations, Khalifa University of Science and Technology, Abu Dhabi 127788, UAE

[#] Chemical Crystallography Laboratory, Khalifa University of Science and Technology, Abu Dhabi, P.O. Box 127788, UAE

[§] Materials and Process Simulation Center (MSC). California Institute of Technology, Pasadena CA 91125, USA

*Email: ahsan.qurashi@ku.ac.ae, Tel: +971 2312 4202

*Email: wag@caltech.edu; 1-626-833-0036

KEYWORDS. Alloy cluster, nanocluster, gram scale synthesis, crystal structure, atomically precise.

Abstract: Although atomically precise noble metal nanoclusters (NMNCs) are highly desirable to unravel the size and structure-activity relationships in catalysis, their synthesis in a controlled way at the atomic level is challenging. Herein, we report the structure and gram scale synthesis of a highly symmetric 2-phenylethanethiol (PETH) and triphenylphosphine (PPh_3)-protected AgCu alloy nanocluster (NC) $[Ag_4Cu_{28}H_6(PET)_{16}Cl_8(PPh_3)_8][BF_4]_2$ with a cuboid shape, denoted as Ag_4Cu_{28}. This was accomplished via a facile one-pot reduction method. Ag_4Cu_{28} NC consists of an Ag_4Cu_4 metal core, six hydrides, four Cu_4Cl_2 units, eight PET ligands, and four $Cu_2(PET)_2(PPh_3)_2$ motifs. High-resolution electrospray ionization mass spectrometry (HRESI MS) and density functional theory (DFT) calculations support this crystal structure. Moreover, Ag_4Cu_{28} exhibits excellent catalytic activity ($k = 7.86\ min^{-1}$) in the hydrogenation of hazardous nitroarenes. This intriguing NC delivers a unique opportunity to explore the gram scale synthesis of alloy nanoclusters and to expand the research on Cu and Ag-based NCs.

1. INTRODUCTION

Ligand-protected noble metal nanoclusters (NMNCs) with specific atomic-level structural features, defined composition, and uniform size have drawn attention of the researchers in materials chemistry and catalysis due to their unique chemical and physical properties.[1-7] NMNCs have the potential to control the activity and product selectivity in various catalytic transformations due to their ultrasmall (typically 3 nm diameter) and tuneable size, coordinated metal sites, unique electronic configuration, metal/ligand composition, and molecular structure.[8-22] They display distinct optical, electrical, dielectric, and magnetic properties.[23-39] Geometry and composition have a significant influence on these unique properties. Several of the properties of these NCs are altered when two or more metals are combined, which frequently increases such desired properties as luminescence and catalysis.[25, 40-44] Investigating the wide range of alloys and their intriguing characteristics is, thus, the primary goal of multicomponent alloy NC research.

Various synthetic methods have been used to create over 300 monometallic NCs of Au, Ag, and Cu.[41] The number of alloy NMNCs, on the other hand, is very low.[41, 45-49] Similarly, the number of alloy clusters with a precise metal core of a single metal is very low. Unlike the rapid expansion of gold and silver alloy clusters, the easy oxidation of copper poses a challenge in the synthesis of stable copper and silver alloy clusters.[8, 41] As a result, the development of a stable copper and silver alloy nanocluster with a defined metal core is much more challenging. The structural data about the core-shell architecture of these alloy NMNCs opens up new possibilities for application development in nanomaterials and improves the understanding of their structure-dependent characteristics.

Herein, we present the gram scale synthesis of an AgCu alloy NMNC, $[Ag_4Cu_{28}H_6(PET)_{16}Cl_8(PPh_3)_8][BF_4]_2$ with a cuboid shape, denoted as Ag_4Cu_{28}, that is stabilized by 2-phenylethanethiol (PETH) and triphenylphosphine (PPh_3) ligands. The crystal structure of the nanocluster was revealed using X-ray crystallography. The crystal structure was supported by ESI MS and density functional theory (DFT) calculations. X-ray photoelectron spectroscopy (XPS) was utilized to confirm the presence of desired elements as well as their oxidation state. The structure of Ag_4Cu_{28} has an Ag_4Cu_4 cubic core. Ag_4Cu_{28} exhibits excellent catalytic activity as a heterogeneous catalyst, with a high reaction rate ($k = 7.86\ min^{-1}$) for the reduction of p-nitrophenol (p-NP) to p-aminophenol (p-AP) using $NaBH_4$.

2. RESULTS AND DISCUSSION

Synthesis, Purification, and Crystallization

Scheme 1. Synthesis of $[Ag_4Cu_{28}H_6(PET)_{16}Cl_8(PPh_3)_8][BF_4]_2$ NC.

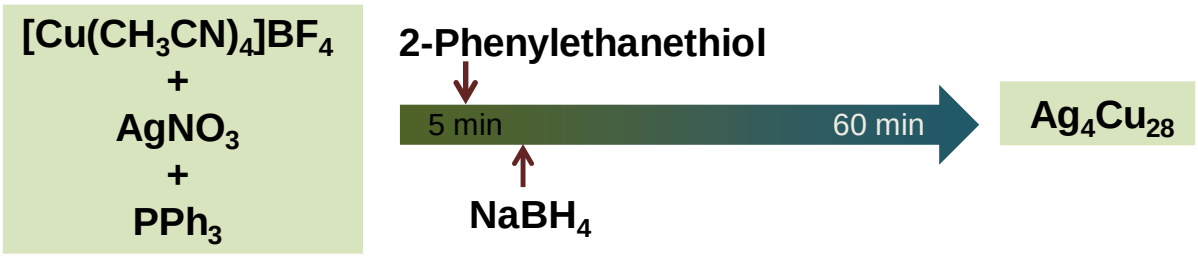

A mixture of Ag and Cu metal precursors was chemically reduced to create Ag_4Cu_{28} NMNCs. In particular, $AgNO_3$ and $[Cu(CN)_4]BF_4$ were reduced using $NaBH_4$ in the presence of the PPh_3 and PETH ligands under ambient conditions (Scheme 1, see the experimental section in supporting information (SI) for more information). These precursors were added to mixed solvents, acetonitrile (CH_3CN) and chloroform ($CHCl_3$). PETH typically serves as the main ligand, interacting with the metal atoms in a variety of coordination modes to stabilize the NC framework.[33] On the other hand, the use of PPh_3 as an auxiliary ligand is advantageous because of its rather rigid and bulky structure, which promotes crystallization of NCs.[33] The above-mentioned chemicals are widely available, which makes it easier to create scalable methods for NC synthesis. It has proven extremely difficult to develop a straightforward, large-scale synthesis approach for NC crystals under ambient conditions because of the extremely sensitive processes involved in the nucleation, development, and crystallization of NCs. The synthesis of pure Ag_4Cu_{28}, which can be produced in large quantities (up to 1.112 g of pure crystals in one pot; Fig. S1) with a good yield (about 35% based on silver), can now be studied in detail, opening up new avenues for applications.[33, 50-52] Within a week, a high-quality dark red crystal (Fig. S1) of Ag_4Cu_{28} was grown in a chloroform/hexane solvent mixture, and single-crystal X-ray diffraction (SCXRD) was used to evaluate its 3D structure.

Crystal Structure and Mass Characterization

The data from SCXRD shows that the Ag_4Cu_{28} NMNCs crystallized in a tetragonal system with the *I*4/*m* space group (Table S1). The two different views of the NC (Fig. 1A and B) revealed that it is made up of 32 metal atoms (silver and copper) with a Ag_4Cu_4 cubic core (occupancy of Ag and Cu in the cubic core is 0.5 and 0.5), eight Cl, sixteen PET, and eight PPh_3 ligands, yielding the chemical formula $[Ag_4Cu_{28}(PET)_{16}Cl_8(PPh_3)_8]^{2+}$ with a cuboid shape.

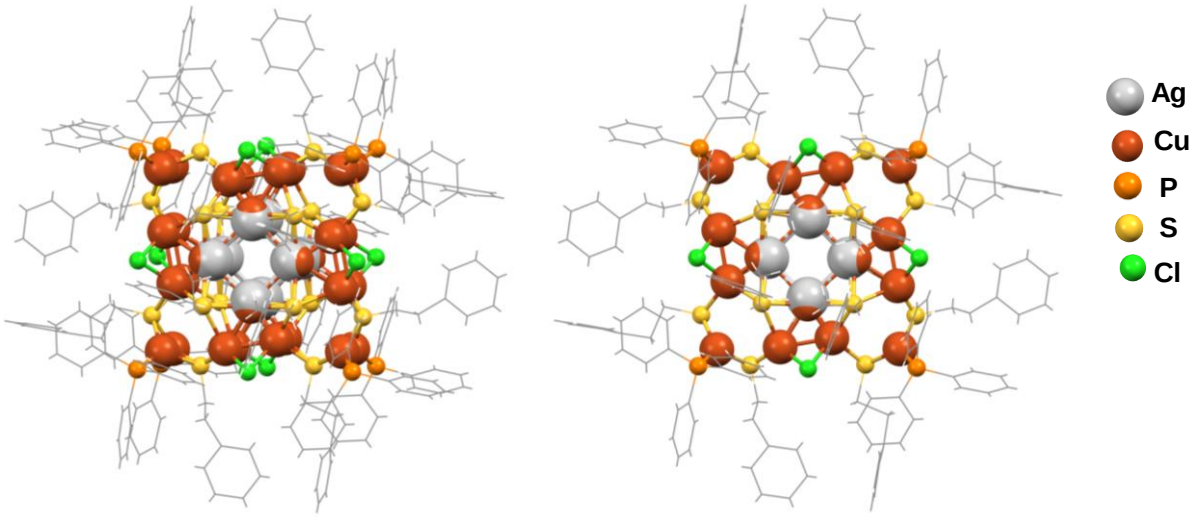

Fig. 1 Crystal structure of Ag_4Cu_{28} NC (Occupancy of Ag and Cu in the cubic core is 0.5 and 0.5). Side-view A) and top-view B) of the Ag_4Cu_{24} NC.

Furthermore, the presence of Ag, Cu, Cl, P, S, and C elements in the Ag_4Cu_{28} cluster was confirmed by X-ray photoelectron spectroscopy (XPS) (Fig. S2). The Cu $2p_{3/2}$ at 932.7 eV and Cu $2p_{1/2}$ at 952.5 eV confirmed the presence of Cu(I).[33] Similarly, Ag $3d_{5/2}$ at 368.7 eV and Ag $3d_{3/2}$ at 374.8 eV indicate the presence of Ag(I). The Cl $2p_{3/2}$ at 198.8 eV and Cl $2p_{1/2}$ at 200.1 eV confirm the presence of Cu-Cl bond. The breaking of carbon-chlorine (C–Cl) bonds in $CHCl_3$ during the reaction process is the source of the Cl^- ions in the structure.[33, 53, 54] We note that the NMNC has some positional disorder, as illustrated in the the supporting crystallographic information file (CCDC 2293022). This type of disorder is frequent in alloy nanoclusters.[8] Note that the structure of Ag_4Cu_{28} in the figures is presented without this disorder.

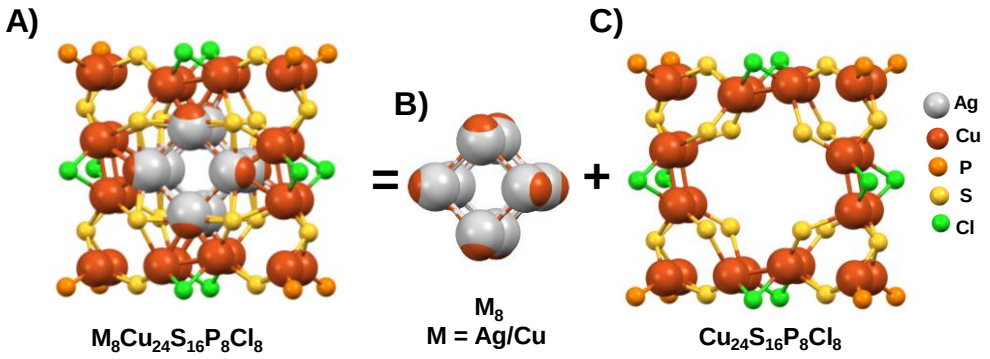

Fig. 2 Crystal structure analysis of Ag_4Cu_{28} NMNC. A) Structure anatomy of the $Ag_4Cu_{28}S_{16}P_8Cl_8$. B) Capping of Ag_4Cu_4 core by C) $Cu_{24}S_{16}P_8Cl_8$.

A comprehensive molecular architecture examination reveals that the Ag_4Cu_{28} cluster has an Ag_4Cu_4 cubic core, as depicted in Fig. 2A and 2B. This cubic Ag_4Cu_4 core is protected by 4 Cu_4Cl_2 units, 8 PET ligands, and 4 $Cu_2(PET)_2(PPh_3)_2$ motifs (Fig. 2A and 2C). The average distance between the central Ag atom and the Cu is 2.705 (4) Å and the average Cu-Cu distance in Cu_4Cl_2 unit is 2.577 (4) -2.745 (5) Å. Each PET ligand in the large surface of the cuboid is bonded with two Ag atoms and two Cu atoms [μ_4-η^1,η^1,(Ag) η^1,η^1(Cu)]. On the other hand, each PET ligand in the small surface of the cuboid is bonded with four Cu atoms (μ_4-η^1,η^1,η^1,η^1). The average distances of Ag-S and Cu-S bonds in AgPET and CuPET are 2.524 (2) Å and 2.315 (4) Å (large surface), respectively. In the 4 $Cu_2(PET)_2(PPh_3)_2$ motifs (Fig. S3A), the average Cu-S and Cu-P distances are 2.294 (4) Å and 2.215 (6) Å, respectively. In the Cu_4Cl_2 unit (Fig. S3B), the average Cu-Cl bond distance is 2.294 (5) Å. We carried out electrospray ionization mass spectrometry (ESI-MS) and DFT calculations to further support the structure because it is very difficult to determine the presence of hydride in NC from SCXRD.[53] The computational details of the DFT calculations are given in the SI.

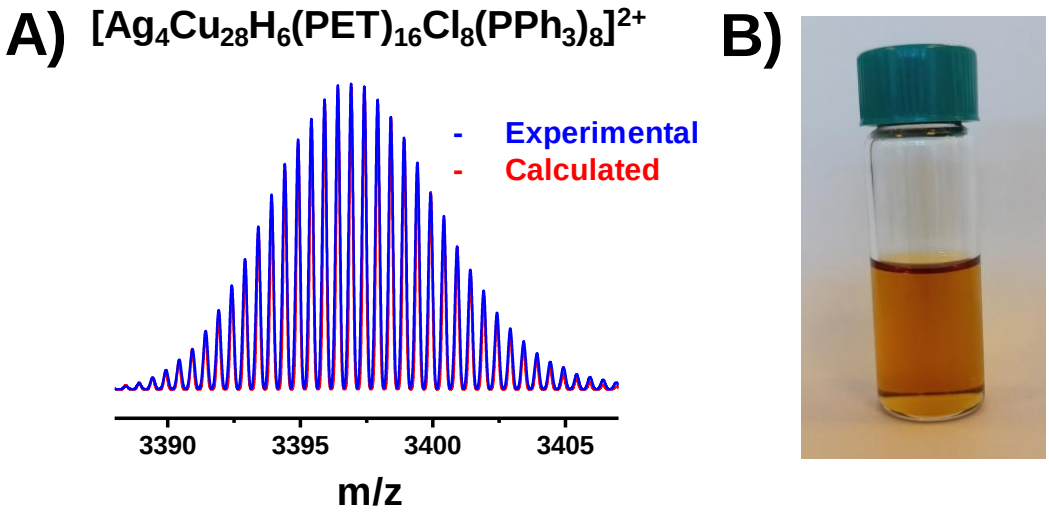

Fig. 3 A) HR-ESI-MS spectrum of Ag_4Cu_{28} NMNC in positive-ion mode after dissolving the crystals in CH_2Cl_2. A comparison of experimental mass spectra of Ag_4Cu_{28} with the simulated is provided. B) Solution of Ag_4Cu_{28} NMNC in CH_2Cl_2.

The Ag_4Cu_{28} NMNC was further analyzed by HRESI-MS to validate the chemical formula acquired from the SCXRD. The mass spectra of Ag_4Cu_{28} revealed a series of peaks in the m/z range 3380 to 3600, as shown in Fig. S4, which may be due to intercluster metal atom exchange under ESI-MS conditions and/or positional disorder of the Ag and Cu atoms.[8] At m/z = 3397, corresponding to the molecular ion Ag_4Cu_{28}. As this peak expands, multiple peaks with a

separation of m/z 0.5 are seen, suggesting that its charge state is 2^+. The peak at m/z 3397 is attributed to a formula $[Ag_4Cu_{28}H_6(PET)_{16}Cl_8(PPh_3)_8]^{2+}$, in agreement with the SCXRD finding, after accounting for all potential elements. The NMNC's hydride ligands are confirmed by comparing the experimental and simulated spectra, which are shown to be in very good agreement (Fig. 3A), further validating this formula assignment. We suggest a formula of $[Ag_4Cu_{28}H_6(PET)_{16}Cl_8(PPh_3)_8]^{2+}$ for the as-synthesized Ag-Cu cluster based on the combined results of SCXRD and ESI-MS. In order to prove the existence of hydrides, a deuterated cluster was created by substituting $NaBD_4$ for $NaBH_4$ as the reducing agent. In fact, Fig. S5 displays a mass spectrum that is upshifted by m/z 2.9 from Ag_4Cu_{28}, indicating a greater mass of 6, thus $[Ag_4Cu_{28}D_6(PET)_{16}Cl_8(PPh_3)_8]^{2+}$ is the composition represented by this upshifted peak. In negative ion mode of the ESI-MS, the presence of BF_4^- was noticed, which suggests that the BF_4^- is acting as a counter anion (Fig. S6). Most significantly, these experimental findings unambiguously imply that the formula of the synthesized NMNC is $[Ag_4Cu_{28}H_6(PET)_{16}Cl_8(PPh_3)_8][BF_4]_2$. The structure is further confirmed by the free valence electron count rule, which indicates that this NMNC has zero free electrons [4+28-6-16-8-2=0]. Fig. 3B shows the color of the NMNC solution in dichloromethane (DCM). The crystals of Ag_4Cu_{28} were stable for six months, which was confirmed by taking ESI-MS of the crystals after dissolving them in DCM (Fig. S7). The Ag_4Cu_{28} NC is also stable in solution for 48 hrs.

Optical Spectrum by DFT

DFT calculations were conducted to optimize the structure from which we predicted the absorbance spectrum. Given the occupancy of Ag and Cu in the cubic core is 0.5 each, we examined three different geometries: (1) Core1 – Ag atoms are connected to Cu atoms and vice versa; (2) Core2 –Ag and Cu atoms are positioned on the same side, and (3) Core3 – an intermediate arrangement between Core1 and Core2 (Fig. 4A and S8). After optimization, Core1 was found to be the most energetically stable, being 1.24 and 1.76 kcal/mol more stable than Core2 and Core3, respectively. This suggests that all 3 configurations are probably present in our samples. In all structures, the cubic Ag_4Cu_4 core was slightly distorted due to different atomic radii of Ag and Cu (Fig. 4A). Among the six hydrides, two are located within the Ag_4Cu_4 core in a μ_4 (μ_4-η^1, η^1, η^1, η^1) form, with Cu-H and Ag-H distances of approximately 1.8 Å and 2.0 Å, respectively. The remaining four hydrides adopt a μ_5 (Ag/Cu-η^1, η^1, Cu-η^1, η^1, η^1) form, with average distances of 1.92 Å for Cu-H and 2.0 Å for Ag-H, respectively (Fig. S8).

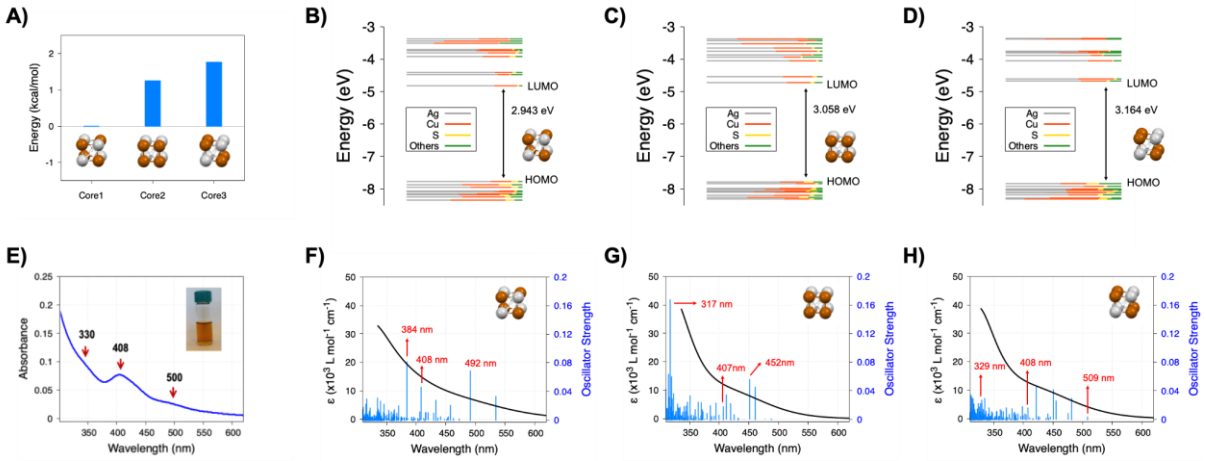

Figure 4. A) Relative energy differences of the three core models with respect to the Core1 model. B-D) KS molecular orbital energy diagrams and the corresponding atomic orbital contributions for each optimized Ag_4Cu_{28} model. E) Experimental UV−vis absorption spectrum of Ag_4Cu_{28} after dissolving the crystals in DCM. F-H) Calculated UV–vis absorption spectra for each model.

The frontier Kohn−Sham (KS) energies and atomic orbital contributions of the optimized Ag_4Cu_{28} models are presented in Figure 4B-D. The HOMO-LUMO energy gaps of Ag_4Cu_{28} were calculated to be 2.943 eV, 3.06 eV, and 3.164 eV for Core1, Core2, and Core3, respectively. The HOMO-LUMO gap of a molecule or its derived descriptor is directly related to its kinetic stability, which is important for synthetic accessibility and isolatability. A small HOMO-LUMO gap indicates strong reactivity as electrons are more easily added to a low-lying LUMO or removed from a high-lying HOMO. In this case, the average HOMO-LUMO energy gap of Ag_4Cu_{28} is larger than Cu_{36} (2.785 eV), suggesting that Ag_4Cu_{28} is more synthetically attainable.[33]

The experimental UV-vis absorption spectrum of Ag_4Cu_{28} exhibits two prominent peaks at 408 and 500 nm, as well as a shoulder peak at 330 nm (Fig. 4E). To investigate the origin of these absorption features, we performed time-dependent DFT (TDDFT) calculations using the optimized structures of three core models (Fig. 4F-H). The excitation around 500 nm was observed for Core1 (492 nm) and Core3 (509 nm), primarily corresponding to electron transitions from the HOMO and HOMO-1 to the LUMO. Transitions involving deeper occupied MO (i.e., orbitals below the HOMO) to unoccupied orbitals (LUMO and higher) are mainly responsible for the higher-energy excitation. Specifically, for the 408 nm absorption peak, all three models showed transitions at similar wavelengths, with Core1 displaying the most intense peak, attributed mainly to a HOMO-4 to LUMO+1 transition. Likewise, all models exhibit

transitions near 330 nm. While these peaks are relatively weak, a strong excitation at 317 nm was observed for Core2, attributed primarily to a HOMO-15 to LUMO+2 transition. Taken together with the small energy differences among the three core models, this absorption analysis suggests that the experimentally synthesized Ag_4Cu_{28} NC is likely a mixture of structures with different core configurations.

Catalytic Hydrogenation of p-nitrophenol

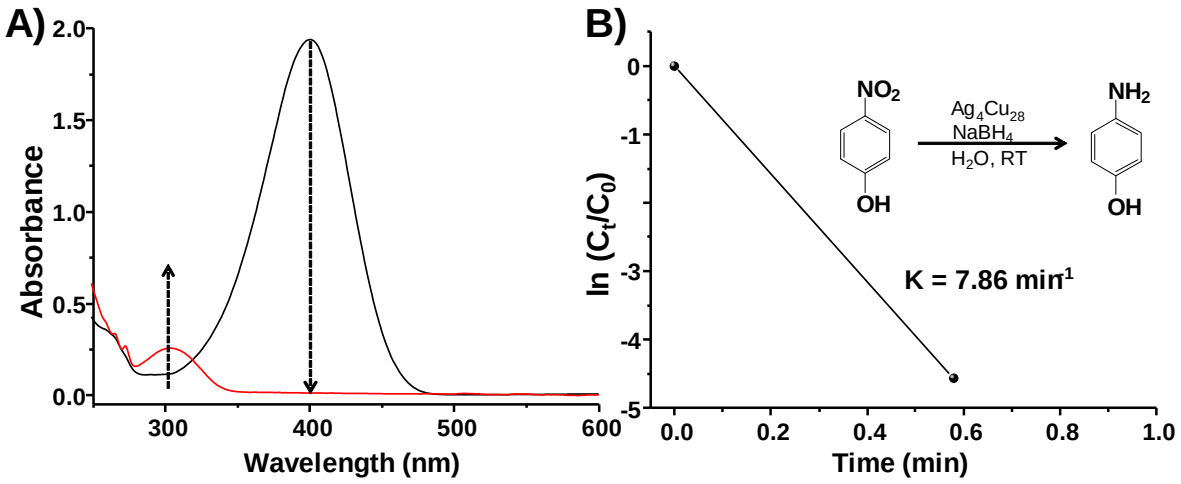

Fig. 5 A) The UV–vis absorption spectra of the catalytic solution as a function of time. B) Plot of $\ln(C_t/C_0)$ versus time for p-NP reduction by $NaBH_4$ aided with catalyst Ag_4Cu_{28}.

The most effective and cost-effective way of getting rid of hazardous nitroaromatics is through catalytic hydrogenation, which can also act as an intermediary for medications and dyes.[55] Furthermore, Ag_4Cu_{28} NC with a good synthetic yield could open the door for further research into the catalytic performance of alloy hydride clusters, a novel class of significant hydrogenation catalysts.[53, 55-57] In light of the aforementioned factors, the model reaction selected to evaluate the activity of Ag_4Cu_{28} NC is the catalytic hydrogenation of p-nitrophenol (p-NP) into p-aminophenol (p-AP) with the assistance of $NaBH_4$.

The reduction process utilizing Ag_4Cu_{28} as the catalyst was simply monitored using time-dependent UV-vis spectroscopy. The intense absorption peak at 400 nm (p-NP) decreases during the catalytic reaction, as shown in Fig. 5A, while a new peak at 300 nm (p-AP) emerges, accompanied by the solution fading from bright yellow to colourless (Fig. S9). At 400 nm

wavelength, the decrease in UV–vis absorption can be approximated as a pseudo-first-order reaction with a rate constant of k = 7.86 min^{-1} (Fig. 5B).[53] Ag_4Cu_{28} exhibited a notably greater catalytic efficiency in comparison (Table S2) to alternative copper hydride catalysts, such as $Cu_{11}H_3(Tf\text{-}dpf)_6(OAc)_2$ ($Cu_{11}H_3$), which achieved complete conversion of p-NP to p-AP in 10 min with k = 0.5 min^{-1}, and $[Cu_{57}H_{20}(PET)_{36}(PPh_3)_4]^+$ in 20 min with k = 0.18 min^{-1}.[55, 58] This suggests that Ag_4Cu_{28} has outstanding activity for catalytic hydrogenation which could be due to the synergistic effects of bimetallic NC. Conversely, the absence of Ag_4Cu_{28} in a blank experiment demonstrated that the p-NP reduction reaction did not occur, as evidenced by the constant absorption spectra after 60 minutes of adding just $NaBH_4$ (Fig. S10).

We conducted a control experiment to investigate deuteration of the Ag_4Cu_{28} NC by reducing 4-NP with $NaBD_4$ and analysing the recovered catalyst using ESI-MS (Fig. S11). HRESI-MS of the Ag_4Cu_{28} after the catalytic reaction suggests that the NMNC is stable under the reaction condition. The ESI-MS analysis after catalysis also revealed that hydrides in the NCs were not replaced by D^- of BD_4^-. This result indicates that the NC's hydrides did not participate directly in the catalytic process, which suggests that the hydrides in BH_4^- were activated on the cluster surface. The hydrides in the NC serve to stabilize the +1 oxidation state of Ag/Cu, holding the cluster together by generating Ag/Cu-H coordination bonds. The electron-deficient Ag(I) and Cu(I) sites in the NC (zero electron count) contribute to its remarkable catalytic performance by promoting hydrogen activation from BH_4^-.[57] Similar kind of reaction mechanism of reduction of 4-NP was studied using AgCu alloy NC.[57, 59].

3. CONCLUSION

In summary, gram scale synthesis of a new AgCu alloy NC $[Ag_4Cu_{28}H_6(PET)_{16}Cl_8(PPh_3)_8][BF_4]_2$ with a cuboid shape co-protected by PETH and PPh_3 ligands was achieved. A variety of characterization techniques were used to determine the overall structure and optical characteristics of the Ag_4Cu_{28}. SCXRD, ESI MS and DFT calculation revealed the presence of a Ag_4Cu_4 core, 6 hydrides, 4 Cu_4Cl_2 atoms, 8 PET ligands, and 4 $Cu_2(PET)_2(PPh_3)_2$ motifs. XPS was used to confirm the elements present in the NC along with their oxidation state. Additionally, Ag_4Cu_{28} exhibits excellent catalytic activity as a heterogeneous catalyst, with a high reaction rate (k = 7.86 min^{-1}) for the reduction of p-NP to p-AP using $NaBH_4$. Our new synthetic strategy for alloy NCs may become a general method to synthesize alloy NCs of other metals with novel crystal structures for various potential applications.

[CCDC 2293022 contains the supplementary crystallographic data for this paper. These data can be obtained free of charge from The Cambridge Crystallographic Data Centre via www.ccdc.cam.ac.uk/data_request/cif.]

Supporting Information

Supporting Information is available from the Online Library or from the author.

Acknowledgements

The author acknowledges Khalifa University of Science and Technology for providing laboratory facilities and instrumentation throughout this research. The authors would like to express their gratitude for the support received from the Center for Catalysis and Separations (CeCaS), AMCC and chemistry department at Khalifa University of Science and Technology. WAG, MYY, and BM were supported by the US National Science Foundation (CBET 2311117).

Notes

The authors declare no competing financial interest.

References

1. J. F. Parker, C. A. Fields-Zinna and R. W. Murray, *Acc. Chem. Res.*, 2010, **43**, 1289-1296.
2. R. Jin, C. Zeng, M. Zhou and Y. Chen, *Chem. Rev.*, 2016, **116**, 10346-10413.
3. I. Chakraborty and T. Pradeep, *Chem. Rev.*, 2017, **117**, 8208-8271.
4. A. Baghdasaryan and T. Bürgi, *Nanoscale*, 2021, **13**, 6283-6340.
5. S. Bonacchi, S. Antonello, T. Dainese and F. Maran, *Chem. Eur. J.*, 2021, **27**, 30-38.
6. P. Chakraborty, A. Nag, A. Chakraborty and T. Pradeep, *Acc. Chem. Res.*, 2019, **52**, 2-11.
7. A. Nag and T. Pradeep, *ACS Nanosci. Au*, 2022, **2**, 160-178.
8. G. Deng, J. Kim, M. S. Bootharaju, F. Sun, K. Lee, Q. Tang, Y. J. Hwang and T. Hyeon, *J. Am. Chem. Soc.*, 2023, **145**, 3401-3407.
9. X.-K. Wan, J.-Q. Wang, Z.-A. Nan and Q.-M. Wang, *Sci. Adv.*, 2017, **3**, e1701823.
10. S. Wang, L. Tang, B. Cai, Z. Yin, Y. Li, L. Xiong, X. Kang, J. Xuan, Y. Pei and M. Zhu, *J. Am. Chem. Soc.*, 2022, **144**, 3787-3792.

11. T. Yoskamtorn, S. Yamazoe, R. Takahata, J.-i. Nishigaki, A. Thivasasith, J. Limtrakul and T. Tsukuda, *ACS Catal.*, 2014, **4**, 3696-3700.

12. S. Lee, M. S. Bootharaju, G. Deng, S. Malola, H. Häkkinen, N. Zheng and T. Hyeon, *J. Am. Chem. Soc.*, 2021, **143**, 12100-12107.

13. X. Cai, G. Saranya, K. Shen, M. Chen, R. Si, W. Ding and Y. Zhu, *Angew. Chem. Int. Ed.*, 2019, **58**, 9964-9968.

14. J. Wang, F. Xu, Z.-Y. Wang, S.-Q. Zang and T. C. W. Mak, *Angew. Chem. Int. Ed.*, 2022, **61**, e202207492.

15. X. Wang, J. Zhao, H. Eliasson, R. Erni, A. Ziarati, S. McKeown Walker and T. Bürgi, *J. Am. Chem. Soc.*, 2023, **145**, 27273-27281.

16. J. Zhao, A. Ziarati, A. Rosspeintner and T. Bürgi, *Angew. Chem. Int. Ed.*, 2024, **63**, e202316649.

17. Y. Zeng, S. Havenridge, M. Gharib, A. Baksi, K. L. D. M. Weerawardene, A. R. Ziefuß, C. Strelow, C. Rehbock, A. Mews, S. Barcikowski, M. M. Kappes, W. J. Parak, C. M. Aikens and I. Chakraborty, *J. Am. Chem. Soc.*, 2021, **143**, 9405-9414.

18. A. Baksi, E. K. Schneider, P. Weis, I. Chakraborty, O. Fuhr, S. Lebedkin, W. J. Parak and M. M. Kappes, *ACS Nano*, 2020, **14**, 15064-15070.

19. Nonappa, T. Lahtinen, J. S. Haataja, T.-R. Tero, H. Häkkinen and O. Ikkala, *Angew. Chem. Int. Ed.*, 2016, **55**, 16035-16038.

20. Nonappa and O. Ikkala, *Adv. Funct. Mater.*, 2018, **28**, 1704328.

21. T. Sengupta, M. Moody, M. Das, A. C. Reber, S. N. Khanna and M. S. El-Shall, *Appl. Catal. A: Gen.*, 2023, **667**, 119448.

22. T. Sengupta, D. Bista and S. N. Khanna, *ACS Catal.*, 2021, **11**, 11459-11468.

23. A. Nag, P. Chakraborty, M. Bodiuzzaman, T. Ahuja, S. Antharjanam and T. Pradeep, *Nanoscale*, 2018, **10**, 9851-9855.

24. L. G. AbdulHalim, M. S. Bootharaju, Q. Tang, S. Del Gobbo, R. G. AbdulHalim, M. Eddaoudi, D.-e. Jiang and O. M. Bakr, *J. Am. Chem. Soc.*, 2015, **137**, 11970-11975.

25. G. Soldan, M. A. Aljuhani, M. S. Bootharaju, L. G. AbdulHalim, M. R. Parida, A.-H. Emwas, O. F. Mohammed and O. M. Bakr, *Angew. Chem. Int. Ed.*, 2016, **55**, 5749-5753.

26. P. Bose, K. Kumaranchira Ramankutty, P. Chakraborty, E. Khatun and T. Pradeep, *Nanoscale*, 2024, **16**, 1446-1470.

27. Y. Wang, X.-H. Liu, R. Wang, B. Cula, Z.-N. Chen, Q. Chen, N. Koch and N. Pinna, *J. Am. Chem. Soc.*, 2021, **143**, 9595-9600.

28. Y. Liu, Z. Li, X.-H. Liu, N. Pinna and Y. Wang, *Nanoscale Horiz.*, 2023, **8**, 1435-1439.

29. P. Chandrashekar, G. Sardar, T. Sengupta, A. C. Reber, P. K. Mondal, D. Kabra, S. N. Khanna, P. Deria and S. Mandal, *Angew. Chem. Int. Ed.*, 2024, **63**, e202317345.

30. S. Biswas, A. K. Das and S. Mandal, *Acc. Chem. Res.*, 2023, **56**, 1838-1849.

31. S. Nematulloev, A. Sagadevan, B. Alamer, A. Shkurenko, R. Huang, J. Yin, C. Dong, P. Yuan, K. E. Yorov, A. A. Karluk, W. J. Mir, B. E. Hasanov, M. Nejib Hedhili, N. M. Halappa, M. Eddaoudi, O. F. Mohammed, M. Rueping and O. M. Bakr, *Angew. Chem. Int. Ed.*, 2023, **62**, e202303572.

32. A. Sagadevan, A. Ghosh, P. Maity, O. F. Mohammed, O. M. Bakr and M. Rueping, *J. Am. Chem. Soc.*, 2022, **144**, 12052-12061.

33. C. Dong, R.-W. Huang, C. Chen, J. Chen, S. Nematulloev, X. Guo, A. Ghosh, B. Alamer, M. N. Hedhili, T. T. Isimjan, Y. Han, O. F. Mohammed and O. M. Bakr, *J. Am. Chem. Soc.*, 2021, **143**, 11026-11035.

34. A. Nag, P. Chakraborty, A. Thacharon, G. Paramasivam, B. Mondal, M. Bodiuzzaman and T. Pradeep, *J. Phys. Chem. C*, 2020, **124**, 22298-22303.

35. W. Kurashige, Y. Niihori, S. Sharma and Y. Negishi, *Coord. Chem. Rev.*, 2016, **320-321**, 238-250.

36. S. Yamazoe, K. Koyasu and T. Tsukuda, *Acc. Chem. Res.*, 2014, **47**, 816-824.

37. S. Knoppe and T. Bürgi, *Acc. Chem. Res.*, 2014, **47**, 1318-1326.

38. X. Yuan, Z. Luo, Y. Yu, Q. Yao and J. Xie, *Chem. Eur. J.*, 2013, **8**, 858-871.

39. X.-R. Song, N. Goswami, H.-H. Yang and J. Xie, *Analyst*, 2016, **141**, 3126-3140.

40. X. Ma, L. Xiong, L. Qin, Y. Tang, G. Ma, Y. Pei and Z. Tang, *Chem. Sci.*, 2021, **12**, 12819-12826.

41. E. Khatun and T. Pradeep, *ACS Omega*, 2021, **6**, 1-16.

42. A. Ghosh, A. Sagadevan, K. Murugesan, S. A. F. Nastase, B. Maity, M. Bodiuzzaman, A. Shkurenko, M. N. Hedhili, J. Yin, O. F. Mohammed, M. Eddaoudi, L. Cavallo, M. Rueping and O. M. Bakr, *Mater. Horiz.*, 2024, **11**, 2494-2505.

43. C. Dong, X. Song, B. E. Hasanov, Y. Yuan, L. Gutiérrez-Arzaluz, P. Yuan, S. Nematulloev, M. Bayindir, O. F. Mohammed and O. M. Bakr, *J. Am. Chem. Soc.*, 2024, **146**, 7373-7385.

44. B. Alamer, A. Sagadevan, M. Bodiuzzaman, K. Murugesan, S. Alsharif, R.-W. Huang, A. Ghosh, M. H. Naveen, C. Dong, S. Nematulloev, J. Yin, A. Shkurenko, M. Abulikemu, X. Dong, Y. Han, M. Eddaoudi, M. Rueping and O. M. Bakr, *J. Am. Chem. Soc.*, 2024, **146**, 16295-16305.

45. J. Yan, H. Su, H. Yang, C. Hu, S. Malola, S. Lin, B. K. Teo, H. Häkkinen and N. Zheng, *J. Am. Chem. Soc.*, 2016, **138**, 12751-12754.

46. H. Yang, Y. Wang, H. Huang, L. Gell, L. Lehtovaara, S. Malola, H. Häkkinen and N. Zheng, *Nat. Commun.*, 2013, **4**, 2422.

47. K. R. Krishnadas, A. Baksi, A. Ghosh, G. Natarajan, A. Som and T. Pradeep, *Acc. Chem. Res.*, 2017, **50**, 1988-1996.

48. X. Kang, S. Wang, Y. Song, S. Jin, G. Sun, H. Yu and M. Zhu, *Angew. Chem. Int. Ed.*, 2016, **55**, 3611-3614.

49. R.-W. Huang, X. Song, S. Chen, J. Yin, P. Maity, J. Wang, B. Shao, H. Zhu, C. Dong, P. Yuan, T. Ahmad, O. F. Mohammed and O. M. Bakr, *J. Am. Chem. Soc.*, 2023, **145**, 13816-13827.

50. A. Chen, X. Kang, S. Jin, W. Du, S. Wang and M. Zhu, *J. Phys. Chem. Lett.*, 2019, **10**, 6124-6128.

51. Y. Song, K. Lambright, M. Zhou, K. Kirschbaum, J. Xiang, A. Xia, M. Zhu and R. Jin, *ACS Nano*, 2018, **12**, 9318-9325.

52. R.-L. He, F. Hu, Z.-J. Guan and Q.-M. Wang, *Angew. Chem. Int. Ed.*, 2024, **63**, e202410827.

53. H. Zhou, T. Duan, Z. Lin, T. Yang, H. Deng, S. Jin, Y. Pei and M. Zhu, *Adv. Sci.*, 2024, **11**, 2307085.

54. A. K. Das, S. Biswas, A. Pal, S. S. Manna, A. Sardar, P. K. Mondal, B. Sahoo, B. Pathak and S. Mandal, *Nanoscale*, 2024, **16**, 3583-3590.

55. G.-G. Luo, Z.-H. Pan, B.-L. Han, G.-L. Dong, C.-L. Deng, M. Azam, Y.-W. Tao, J. He, C.-F. Sun and D. Sun, *Angew. Chem. Int. Ed.*, 2023, **62**, e202306849.

56. S. Lee, M. S. Bootharaju, G. Deng, S. Malola, W. Baek, H. Häkkinen, N. Zheng and T. Hyeon, *J. Am. Chem. Soc.*, 2020, **142**, 13974-13981.

57. S.-F. Yuan, Z.-J. Guan and Q.-M. Wang, *J. Am. Chem. Soc.*, 2022, **144**, 11405-11412.

58. C.-Y. Liu, S.-F. Yuan, S. Wang, Z.-J. Guan, D.-e. Jiang and Q.-M. Wang, *Nat. Commun.*, 2022, **13**, 2082.

59. H. Guo, Y. Chen, Y.-Z. Han, Q. Wu, L. Wang, Q. Xu, R. Huo, X. Gong, J. Sun, Q. Tang and H. Shen, *Chem. Mater.*, 2024, **36**, 7243-7251.